GFZ
Helmholtz-Zentrum
POTSDAM

Originally published as:

Biedermann, N., Speziale, S., Winkler, B., Reichmann, H.-J., Koch-Müller, M., Heide, G. (2017): High-pressure phase behavior of SrCO3: an experimental and computational Raman scattering study. - *Physics and Chemistry of Minerals*, *44*, 5, pp. 335—343.

DOI: http://doi.org/10.1007/s00269-016-0861-2

Title: High-pressure phase behavior of $SrCO_3$: an experimental and computational Raman scattering study

Authors and affiliations:

Nicole Biedermann[1]

Sergio Speziale[1]

Björn Winkler[2]

Hans Josef Reichmann[1]

Monika Koch-Müller[1]

Gerhard Heide[3]

[1]GFZ German Research Center for Geosciences, Section 4.3, Potsdam, Germany,

[2]Institute for Geosciences, Goethe University, Frankfurt am Main, Germany

[3]Institute for Mineralogy, TU Bergakademie Freiberg, Freiberg, Germany

Corresponding author:

Nicole Biedermann, GFZ German Research Center for Geosciences, section 4.3, Telegrafenberg, 14473 Potsdam, Germany, nicole.biedermann@gfz-potsdam.de, Tel. +49 (0)331/288 - 27510

Abstract

The high-pressure phase behavior of strontianite ($SrCO_3$) was both experimentally and theoretically investigated by Raman spectroscopy up to 78 GPa in a diamond anvil cell and density functional theory-based calculations. Our study shows a phase transition between 23.7 and 26.8 GPa during compression from space group *Pmcn* to post-aragonite $SrCO_3$, which is accompanied by significant changes in the vibrational spectrum. The excellent agreement between the observed and computed Raman frequencies and intensities implies that the high-pressure polymorph has space group *Pmmn* and contributes to resolving an existing disagreement concerning the correct space group symmetry of this high-pressure polymorph. It is shown that the transition pressure from the aragonite to a post-aragonite phase increases linearly with decreasing cation radius for (Ca, Sr, Ba, Pb) carbonates.

Keywords

$SrCO_3$ · High pressure · Phase transformation · Diamond anvil cell · DFT calculations

Introduction

Carbonates are key phases which control the carbon cycle in the interior of our planet. They are important crustal materials but also present in the deep Earth. Experimental data indicate that under the P-T-conditions of the upper mantle CO_2 is not present as a fluid and carbonates are therefore the major carriers of oxidized carbon into the deep mantle (Kushiro et al. 1975; Biellmann et al. 1993; Kerrick and Connolly 2001; Dasgupta and Hirschmann 2010; Hammouda and Keshav 2015). In addition, analyses of inclusions in transition-zone diamonds were taken as evidence for the presence of carbonates in the lower mantle region (Brenker et al. 2007). Accordingly, understanding the physical properties of carbonate minerals and their high-pressure behavior is a major focus of mineral physics research and is required to decipher the dynamics of carbon cycling in the Earth's mantle.

Natural carbonates are solid solutions with the general formula XCO_3, where X is a divalent cation such as Mg^{2+}, Ca^{2+}, Sr^{2+}, Ba^{2+} , Pb^{2+}, Fe^{2+} or Mn^{2+} (Deer et al. 1992). Calcite, $CaCO_3$, as the most abundant carbonate phase in crustal materials, undergoes several high-pressure phase transitions (e.g., Merlini et al. 2012). Aragonite, one of the high-pressure polymorphs of calcite, has an orthorhombic symmetry (space group *Pmcn*) with Z = 4 formulae per unit cell (Fig. 1a). The structure is characterized by planar trigonal $[CO_3]^{2-}$ complexes oriented parallel to the *c*-axis and a ninefold coordinated cation (De Villiers 1971). Carbonates containing cations larger than Ca^{2+} (e.g., Sr, Ba, Pb) crystallize in the aragonite structure at ambient conditions, whereas carbonates with cations smaller than Ca^{2+} crystallize in the calcite structure. With increasing pressure, carbonates in the aragonite structure are not stable anymore and transform into the so-called post-aragonite structure type (e.g., Lin and Liu 1997a). According to the pressure-coordination rule (Neuhaus 1964), the coordination number of the cation is expected to increase from 9 to a higher value across the pressure-induced transition into the post-aragonite phase. $SrCO_3$ is often present as a major component in natural aragonite and in biogenic aragonite with up to 2 mol% (Milliman 1974). The knowledge of the properties and high-pressure phase behavior of the $SrCO_3$ chemical component is therefore important for a quantitative understanding of the thermodynamics of complex carbonates. In addition, a better characterization of this phase transition certainly helps us to expand our knowledge of the systematics of pressure-induced changes in carbonates.

There are several studies of high-pressure phase transitions in aragonite-group minerals, but their results do not yet furnish a completely consistent picture of their phase diagrams. Lin and Liu (1997b) suggested a phase transition to a post-aragonite phase of $SrCO_3$ between 32 and 35 GPa at ambient temperature. Based on their analyses of quenched high-pressure polymorphs of $SrCO_3$, $PbCO_3$ and $BaCO_3$, they proposed that all high-pressure polymorphs have the same crystal structure with space group $P2_122$. Ono et al. (2005) observed a new post-

aragonite phase of $SrCO_3$ already at 10 GPa of a quenched sample that was heated up to 1500 K in order to relax the differential stress. Later, Ono (2007) performed the similar experiments with $BaCO_3$ and concluded that the orthorhombic symmetry of a post-aragonite structure of $BaCO_3$ between 10 and 24 GPa is identical to that of the corresponding post-aragonite phases of $CaCO_3$ and of $SrCO_3$. Based on first-principle electronic structure calculations, Arapan and Ahuja (2010) concluded by using experimental results from Ono et al. (2005) that the transition pressures for an aragonite to a post-aragonite phase with space group symmetry *Pmmn* for $CaCO_3$, $SrCO_3$ and $BaCO_3$ are 42, 17 and 7 GPa, respectively. In a recent experimental study, using either silicon oil or methanol-ethanol as a pressure transmitting medium Wang et al. (2015) reported a pressure-induced transition of $SrCO_3$ from the aragonite structure *Pmcn* to $P2_12_12$ between 22.2 and 26.9 GPa at ambient temperature. Hence, the proposed transition pressures for the aragonite to post-aragonite transition for $SrCO_3$ range from 10 to 35 GPa and the space group symmetry of the high-pressure phase is still under debate.

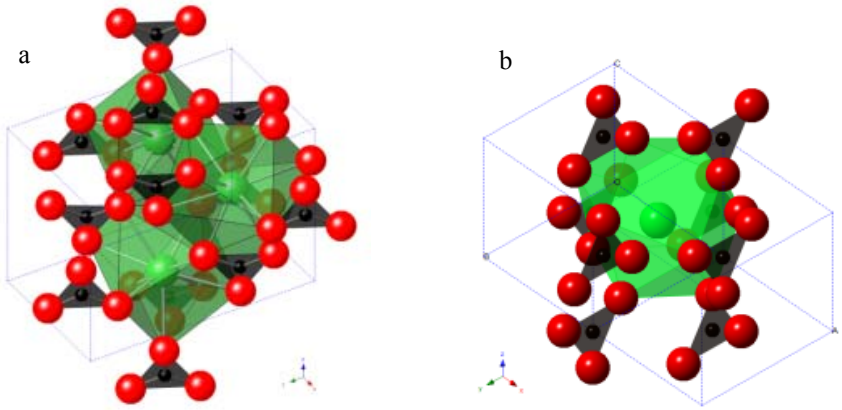

Fig. 1: Structural model and coordination polyhedra for aragonite (a) and post-aragonite (b) phase of $SrCO_3$. The low-pressure phase of $SrCO_3$ has space group *Pmcn* and is characterized by a ninefold coordination for the cation, e.g., Sr^{2+}, whereas the high-pressure phase of $SrCO_3$ has a *Pmmn* structure with 12-fold coordinated Sr^{2+} and is observed above 23.7 GPa at room temperature

We have investigated the high-pressure phase behavior of synthetic $SrCO_3$, up to 78 GPa by Raman spectroscopy to further constrain the high-pressure behavior of aragonite-structured carbonates. Raman spectroscopy is a very useful tool for this purpose because it is sensitive toward structural changes, and the irreducible representations for the aragonite-type structure are Γ_{tot}= 9 A_g (R) + 6 B_{1g} (R) + 9 B_{2g} (R) + 6 B_{3g} (R) + 6 A_u (IR) + 8 B_{1u} (IR) + 5 B_{2u} (IR) + 8 B_{3u} (IR) (Frech et al. 1980) of which 30 modes are Raman active, namely the 9 A_g, 6 B_{1g}, 9 B_{2g} and 6 B_{3g} modes. Up to now, only a single Raman spectroscopic study of $SrCO_3$ at high pressures was performed by Lin and Liu (1997b) in which water was used as a pressure-transmitting medium. However, water

crystallizes into ice at 0.93 GPa and ambient temperature. In our experiments, we have used argon as a pressure-transmitting medium, which provides a significantly more hydrostatic environment. We have complemented the experimental study with density functional theory (DFT)-based calculations and have therefore been able to quantitatively interpret the pressure-induced structural and spectroscopic changes.

Experimental

Strontianite was synthesized at 4 GPa and 1273 K for 24 hours in a multi-anvil apparatus based on the design developed by Walker et al. (1990) in order to form single crystals of pure $SrCO_3$ of sizes up to 500 µm. As a starting material, $SrCO_3$ powder from *Sigma-Aldrich Chemical Company* with a nominal purity of 99.995% strontium carbonate was employed. We intentionally did not remove traces of adsorbed water in the starting material as this may have served as a flux to enhance the growth of large crystals. Microprobe analysis showed that the synthetic crystals are chemically pure with a concentration of Ca^{2+} below the detection limit of 130 ppm. In addition, the sample material was characterized by powder X-ray diffraction using a STOE Stadi P diffractometer with a primary monochromator and Cu-$K\alpha_1$-radiation. The results confirm that the synthesis products are strontianite. The lattice parameters of our sample material are a = 5.103(4) Å, b = 8.407(7) Å and c = 6.022(5) Å. These lattice parameters are in excellent agreement with published data (Speer and Hensley-Dunn 1976). To perform high-pressure experiments, the samples (either as a single crystal or as a powder) were pressurized using a symmetric piston-cylinder diamond anvil cell (Mao et al. 1997) with 300-µm culets. The sample material and a ruby sphere were placed into a 150-µm-wide cylindrical chamber drilled in a preindented rhenium gasket. Liquid argon was loaded cryogenically into the cell as a pressure-transmitting medium. The pressure in the cell was measured using the ruby fluorescence method (Mao et al. 1986). The spectrometer used in this study is a HORIBA Jobin-Yvon LabRam HR800 Vis Raman spectrometer equipped with a Synapse® 2048 x 512 back-illuminated CCD detector. The grating had 1800 lines/mm, the slit aperture was set to 500 µm, and the confocal pinhole had a diameter of 50 µm. The *LabRam* system is equipped with an optical microscope and an Olympus SLMPlan 20x objective (numerical aperture 0.25). A confocal system (Minsky 1961) is used to increase the optical resolution. We used a blue diode-pumped solid-state laser (DPSS laser) with a wavelength of 473 nm, and the laser power measured downstream of the objective was 12 mW. Unpolarized Raman spectra of $SrCO_3$ were obtained by averaging three measurements of 120-s duration at low pressures (up to 22 GPa) and ten measurements of 180-s at high pressures. In addition, spectra were also recorded at each pressure simultaneously with the emission lines of a neon lamp to calibrate the positions of the observed Raman bands. The software PeakFit

version 4.11 by SYSTAT Software Inc. was used for data analysis. A linear baseline was subtracted and symmetric peak shapes (Gaussian + Lorentzian area model) were used to fit the positions of the Raman modes. More than 70 spectra were recorded at ambient temperature and pressures up to 78.5 GPa. Additional spectra were collected on pressure decrease.

Computational methods

DFT calculations were done with commercial and academic versions of the CASTEP program (Clark et al. 2005) using the generalized gradient approximation (GGA) formalized by Perdew-Burke-Ernzerhof (PBE) (Perdew et al. 1996) with a plane-wave basis set and qc-optimized norm-conserving pseudopotentials (Rappe et al. 1990). The maximum cutoff energy of the plane waves was 900 eV. An 8 × 4 × 6 Monkhorst-Pack grid (Monkhorst and Pack 1976) was employed for sampling of reciprocal space corresponding to a k-point separation of less than 0.030 $Å^{-1}$. Raman shifts and intensities were obtained within the formalism of harmonic ab initio lattice dynamics using density functional perturbation theory (DFPT) (Refson et al. 2006) for pressures up to 70 GPa with trial structures derived from earlier publications. The computed Raman spectra were artificially broadened in order to mimic an instrumental resolution function of 5 cm^{-1}. This approach has been validated by an extensive comparison to ambient pressure Raman and IR data, low-temperature heat capacities, thermal diffuse and inelastic X-ray scattering experiments (Nguyen-Thanh et al. 2016).

Results

Selected Raman spectra in the frequency regions 100–850, 1050–1250 and 1440–1600 cm^{-1} are presented in Figs. 2, 3 and 4, as a function of pressure. The pressure shifts of the fitted mode frequencies are listed in Tables 1 and 2 and are shown in Figs. 5 and 6. From these figures, it is clear that there is a discontinuous change in the spectra at ~23-25 GPa, indicating the onset of a pressure-induced structural phase transition. The changes include both the appearance of new modes and a discontinuous change in the mode Grüneisen parameters (see supplemental data set for calculated mode Grüneisen parameter γ_i).

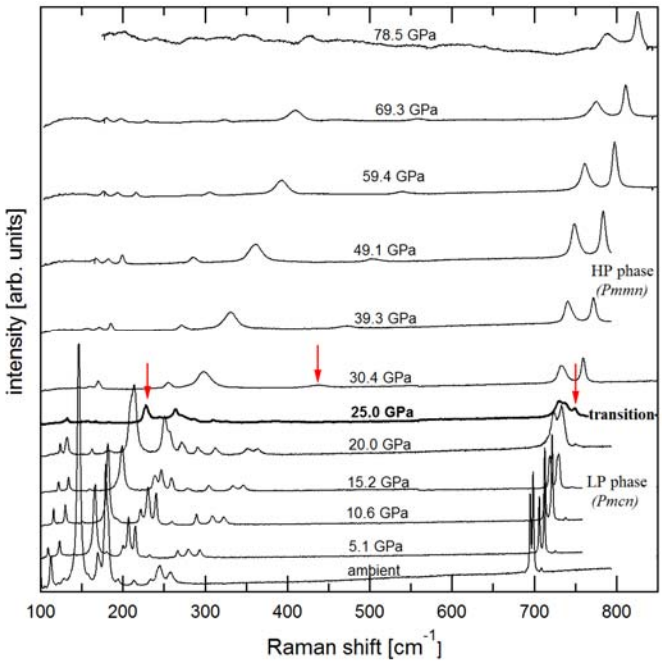

Fig. 2: Selected Raman spectra during compression of the Raman modes of $SrCO_3$ in the low frequency range between 100 and 850 cm^{-1} as a function of pressure. The arrows indicate the appearance of new Raman bands that are attributed to the high-pressure phase of $SrCO_3$

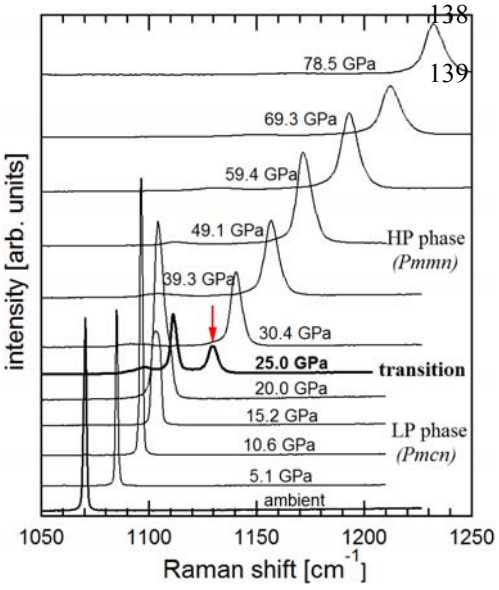

Fig. 3: Selected Raman spectra of the Raman modes of $SrCO_3$ in the 1050-1250 cm^{-1} frequency range as a function of pressure. *Arrow* indicates the appearance of a new Raman band attributed to the high-pressure phase of $SrCO_3$

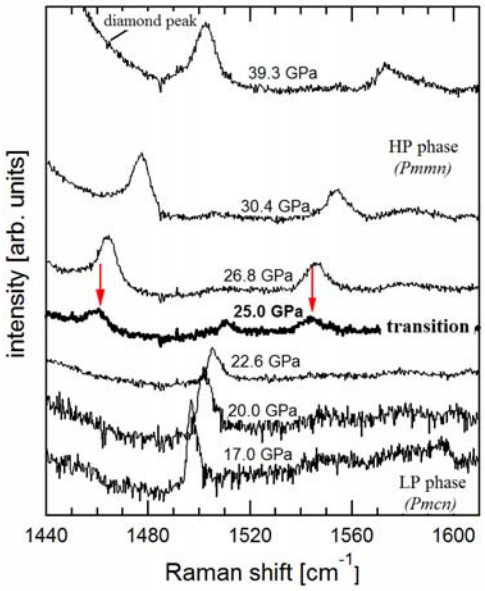

Fig. 4: Raman spectra of the Raman modes in the 1440-1600 cm^{-1} frequency range between 17.0 and 39.3 GPa. *Arrows* indicate the appearance of new Raman bands that are attributed to the high-pressure phase of $SrCO_3$. Above 39.3 GPa, a diamond peak is overlapping the Raman signal of strontianite

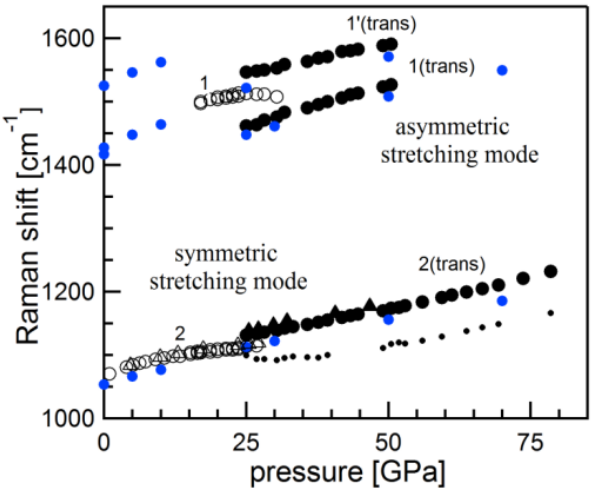

Fig. 5: Pressure dependence of $SrCO_3$ Raman modes frequencies in the range between 1000 and 1600 cm^{-1} measured in quasi-hydrostatic conditions and at ambient temperature. Modes of the low-pressure phase are labeled with *numbers* and are displayed with *open symbols*, whereas high-pressure modes are represented by *filled symbols*. Additional results from powder experiments are marked with *triangles*. Calculated Raman frequencies are plotted as *blue filled circles*

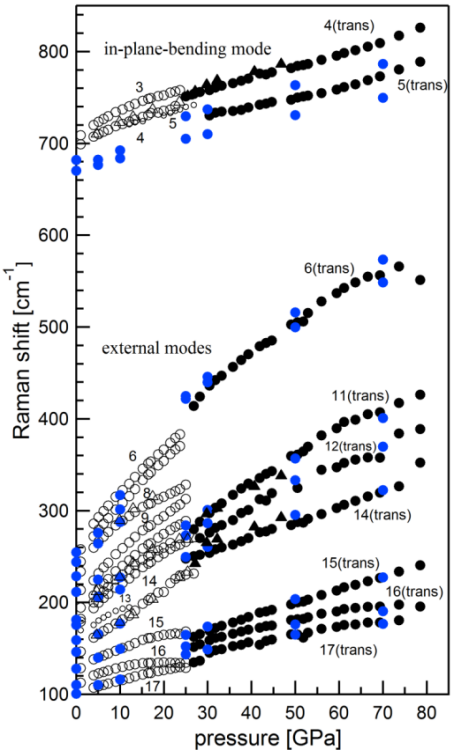

Fig. 6: Pressure dependence of frequencies of the Raman modes of $SrCO_3$ in the low frequency range between 100 and 850 cm^{-1} under quasi-hydrostatic conditions and at ambient temperature. For symbols definition, see Fig. 5

On compression, the aragonite and post-aragonite phases coexist between 23.7 and 26.8 GPa. The appearance of new modes indicates a symmetry change, and the coexistence implies that the transition is of first order. The pressure gradient in the cell is supposed to be well below the resolution of the Raman pressure calibration, of approximately 0.2 GPa (Müller et al. in press), and does not affect the phase transition in $SrCO_3$.

In Fig. 7, a comparison between our experimentally determined and calculated Raman spectra for selected pressures is visible. Seventeen Raman modes out of the predicted 30 Raman-active modes can be observed at very low pressures. The systematic deviation between experimentally determined and computed frequencies in the ambient pressure spectra has already been discussed by Nguyen-Thanh et al. (2016). The deviations are small (a few percent) and are due to the approximations made in the quantum mechanical calculations and the influence of temperature, which is neglected in the calculations. Inspection shows that the intensity ratios are reproduced very well, and an unambiguous symmetry assignment of the Raman modes is therefore feasible (see Tables 1, 2).

The DFT-based calculations showed that the low-pressure phase *Pmcn* is stable to about 20 GPa. At 25 GPa, a polymorph with space group symmetry *Pmmn* became stable. Geometry optimizations starting with space group symmetry $P2_12_12$ converged to the *Pmmn* structure. The high-pressure structure is characterized by planar trigonal CO_3^{2-} groups perpendicular to (100) and an increase in the coordination of the cations from ninefold to a 12-fold (Fig. 1b). The irreducible representations of a phase with *Pmmn*-symmetry with two formula units in the unit cell are $\Gamma_{tot} = 5\ A_g\ (R) + 2\ B_{1g}\ (R) + 6\ B_{2g}\ (R) + 5\ B_{3g}\ (R) + A_u + 3\ B_{1u}\ (IR) + 2\ B_{2u}\ (IR) + 3\ B_{3u}\ (IR)$. A comparison of the theoretical spectra with the experimentally determined spectra shows that the DFT-based model calculations reproduce the phonon frequencies and the relative Raman intensities for the high-pressure spectrum with the same accuracy as for the ambient pressure spectrum (Fig. 7). The excellent agreement of theoretical and experimental frequencies and relative intensities implies that the high-pressure polymorph has a structure of space group *Pmmn*. Therefore, it is now possible to unambiguously perform a symmetry assignment to the high-pressure spectra.

On decompression, the *Pmmn* structure of $SrCO_3$ reverts back to the aragonite structure below 18.0 GPa. A significant hysteresis is characteristic for first-order structural phase transition.

Table 1: Experimentally observed strong Raman modes for *Pmcn*-$SrCO_3$ during compression (see open symbols in Figs. 5, 6) and their linear pressure shifts

ω_0 (cm^{-1}) obs. (calc.)	Assignment	Raman line	$d\omega/dP$ (cm^{-1}/GPa)
(1467)	$\nu_3(A_g)$	1	2.0(1)
1070 (1069)	$\nu_1(A_g)$	2	1.5(1)
709 (707)	$\nu_4(B_{1g})$	3	3.50(9)[a]
699 (701)	$\nu_4(A_g)$	4	1.79(6)
(703)	$\nu_4(B_{2g})$	5	1.44(5)
258 (256)		6	7.2(3)[a]
244 (242)		7	7.2(3)[a]
234 (234)		8	6.3(4)[a]
213 (206)		9	5.5(2)[a]
194 (188)		10	5.57(8)[a]
182 (178)	External modes	11	6.0(2)[a]
179 (174)		12	4.96(9)[a]
170 (166)		13	3.2(5)[a]
146 (147)		14	3.37(7)
128 (126)		15	2.9(1)[a]
113 (112)		16	2.4(1)[a]
100 (102)		17	1.18(5)

[a] Linear shift at ambient pressure derived from a quadratic fit

Table 2: Experimentally observed strong Raman modes for $SrCO_3$ with a post-aragonite structure *Pmmn* during compression (see filled symbols in Figs. 5, 6) and their linear pressure shifts.

ω_{27GPa} (cm^{-1}) obs. (calc)	Assignment	Raman line	$d\omega/dP$ (cm^{-1}/GPa)[a]
1548 (1548)	$\nu_3(B_{2g})$	1'(trans)	1.85(6)
1463 (1467)	$\nu_3(A_g)$	1(trans)	2.60(6)
1134 (1132)	$\nu_1(A_g)$	2(trans)	1.83(3)
754 (754)	$\nu_4(A_g)$	4(trans)	1.33(2)
742 (725)	$\nu_4(B_{2g})$	5(trans)	1.1(4)
414 (430)		6(trans)	3.0(1)
280 (291)		11(trans)	2.87(8)
(272)	External modes	12(trans)	2.29(7)
250 (248)		14(trans)	1.73(5)
163 (165)		15(trans)	1.48(1)
151 (156)		16(trans)	1.00(4)
135 (141)		17(trans)	0.97(4)

All Raman modes that were assigned to the high-pressure polymorph of $SrCO_3$ are marked with "trans"

[a] $d\omega/dP$ determined between 27 and 78 GPa (see also supplemental material)

Discussion and conclusions

The combination of experimental and computational results of our study clearly shows a transition from strontianite to a post-aragonite phase with space group *Pmmn*. We think that in the absence of a convincing demonstration of acentricity, e.g., by high-pressure second-harmonic-generation experiments (Bayarjargal and Winkler 2014), diffraction experiments carried out in significantly non-hydrostatic environments in a DAC lack the required accuracy to provide the basis for a reliable structure refinement in an acentric space group. We find that the high- and low-pressure phases of strontianite coexist between 23.7 and 26.8 GPa. This is in between the experimental range of 32-35 GPa published by Lin and Liu (1997b) and the theoretical data of 17 GPa by Arapan and Ahuja (2010), and in agreement with the pressure range given by Wang et al. (2015) who reported a range of 22- 27 GPa. The experiments of Ono et al. (2005) cannot be compared directly to our results because they used a different method to investigate the phase transition and the sample was heated up to overcome a kinetic barrier.

The transition pressure observed in our Raman scattering experiments (between 23.7 and 26.8 GPa) agrees with our DFT computations (20–25 GPa). However, theoretical DFT-based transition pressures strongly depend on the exchange-correlation functional employed. As the calculations are generally done in the athermal limit, the influence of temperature is neglected. On the other hand, non-hydrostaticity in the experiments may shift the transition pressure in structural phase transitions by several GPa (Bayarjargal and Winkler 2014), the microstructure may play a role, and reconstructive phase transitions may be kinetically hindered. It is therefore typical that theoretical transition pressures deviate from experimental values and a comparison is not straightforward. The discrepancy between the data published by Lin and Liu (1997b) and the transition pressure obtained here is probably due to their use of a natural strontianite with a composition of $(Sr_{0.86}Ca_{0.14})CO_3$, i.e., with a significant amount of Ca^{2+} in the structure, and the strongly non-hydrostatic conditions in their DAC due to the use of water as a pressure-transmitting medium (Bayarjargal and Winkler 2014).

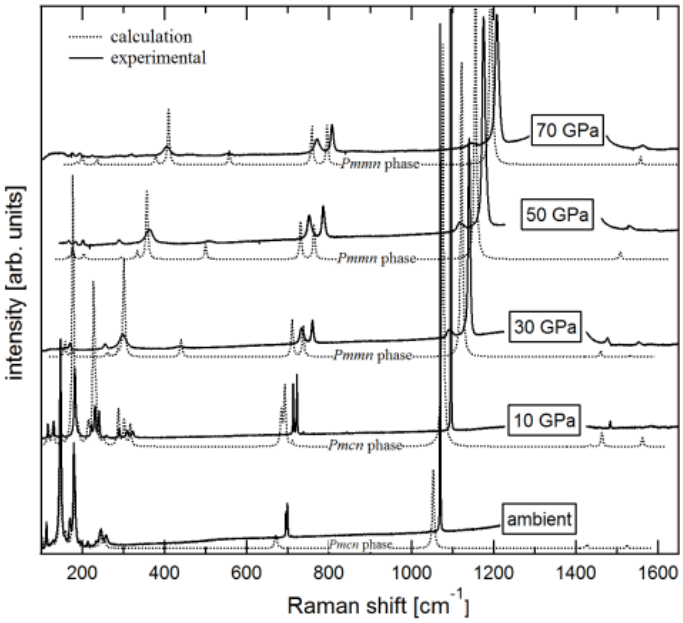

Fig. 7: Calculated and experimental Raman spectra at ambient pressure, 10, 30, 50 and 70 GPa. The low-pressure phase strontianite has aragonite-type structure with space group *Pmcn*. Calculations confirm that the most stable structure of the high-pressure phase of $SrCO_3$ has an orthorhombic structure with space group *Pmmn*. The theoretical Raman shifts have not been scaled

The number of Raman spectroscopic studies on aragonite-type carbonates at high pressures that can be compared to our study is limited. We complemented our data set for $SrCO_3$ with calculated Raman spectra of $BaCO_3$ and $PbCO_3$ at 30 GPa. All three aragonite-type carbonates follow the same phase transition as the number of vibrational frequencies at high pressure is the same (Fig. 8; Table 3). We first ensured the reliability of our model calculations, for both the ambient pressure and the high-pressure phases. We found the same accuracy as for the $SrCO_3$ calculations. As an example, in Fig. 9 we compare a part of the Raman spectrum of $BaCO_3$, measured at 22.3 GPa by Chaney et al. (2015), with our calculations. As is nearly always the case, the theoretical spectrum is systematically shifted, and here we have scaled the computed Raman shifts by 6%. This is a typical value required to achieve a good agreement between experiment and theory (Bosak et al. 2009). The Raman spectra of the three carbonates in Fig. 8 are, as expected, similar. The differences are mainly due to the different atomic masses and nicely illustrate the fact that the polarization vectors rarely correspond to a motion which can be described purely in terms of a simple distortion of a group of atoms, such as the "asymmetric stretching vibration of the CO_3^{2-} units," but instead that cation substitution influences all Raman bands to some extent.

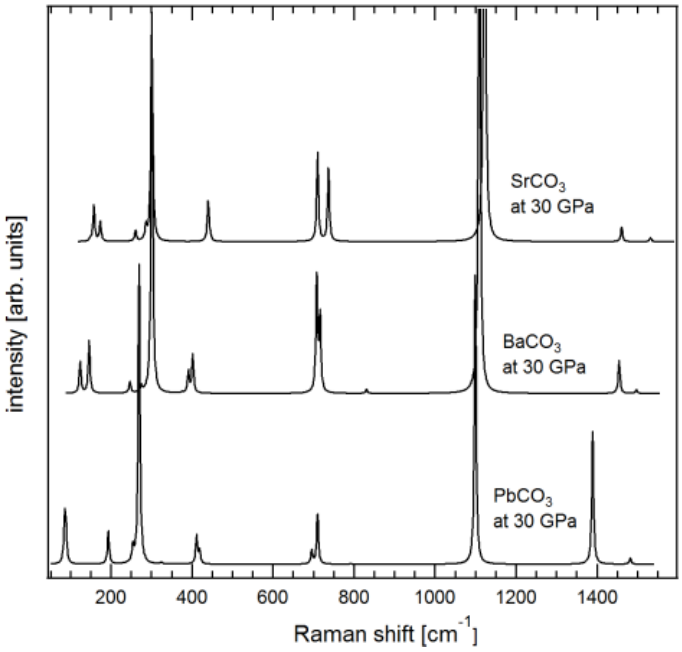

230

231 **Fig. 8: Calculated Raman spectra for $SrCO_3$, $BaCO_3$ and $PbCO_3$ with post-aragonite structure *Pmmn* at 30 GPa**

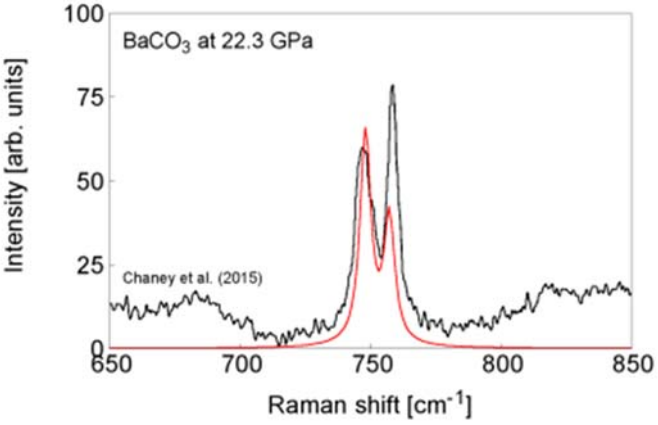

232

233 **Fig. 9: Experimental (Chaney et al. 2015) and theoretical (this study) Raman spectrum of $BaCO_3$ at 22.3 GPa. The**
234 **theoretical Raman shifts have been scaled by 6% in order to compensate for deficiencies in the model calculations, i.e.,**
235 **the neglect of temperature and anharmonicity. The experimentally determined intensities suffer from a poor sampling**
236 **statistics and preferred orientation of the sample in the diamond anvil cell**

237

Table 3: Comparison of the experimentally observed and calculated Raman modes for the aragonite-group minerals $SrCO_3$, $BaCO_3$ and $PbCO_3$ in the post-aragonite structure P*mmn*

Assignment	P*mmn*-$SrCO_3$ this study (calc.)	P*mmn*-$BaCO_3$ Chaney et al. 2015 (calc.)		P*mmn*-$PbCO_3$ Minch et al. 2010 (calc.)	
	At 30 GPa	At 22.3 GPa	At 30 GPa	At 10 GPa	At 30 GPa
$\nu_3(B_{2g})$	1553 (1532)	1456 (1481)	(1497)	(1435)	(1482)
$\nu_3(A_g)$	1475 (1461)	1390 (1433)	(1455)	(1335)	(1389)
$\nu_1(A_g)$	1139 (1122)	1074 (1095)	(1109)	1081(1061)	(1099)
$\nu_2(B_{2g})$			(831)	827	
$\nu_4(A_g)$	758 (737)	708 (708)	(716)	691(686)	(710)
$\nu_4(B_{2g})$	731 (710)	701 (699)	(708)	708	(696)
External modes	(446)	(375)	(402)	(344)	(419)
	436 (440)	(360)	(391)	(327)	(411)
	297 (301)	(275)	(301)		(325)
	276 (286)	(254)	(275)	(193)	(269)
	254 (261)	183 (230)	(247)	(183)	(254)
	169 (174)	177	(146)	(134)	(194)
	159 (158)	96 (134)	(124)		(87)
	145 (149)	87 (118)			

Raman modes are given in cm^{-1}

As mentioned in "Introduction", isostructural compounds often exhibit similar phase transition sequences where the transition pressures are shifted to lower pressures with increasing ionic radius according to the pressure-homologue rule (Neuhaus 1964; Ringwood 1975). In that sense, $SrCO_3$ is an analogue material to understand $CaCO_3$ at conditions which are present in the deep Earth. A summary of the transition pressures for all aragonite-type carbonates is shown in Fig. 10 and suggests a linear relationship between cation radius and transition pressure. Note that some experimental results reported in Fig. 10 are based on experiments with annealed samples at high pressure to overcome potential kinetic hindrance of the phase transitions. The phase transition in $PbCO_3$ occurs at slightly lower pressure than the linear trend which might be related to the fact that Pb^{2+} has a substantially different electronic configuration (Siidra et al. 2008; Minch et al. 2010) compared to the alkaline earth elements (i.e., Ca, Sr, Ba). The transition pressure for $SrCO_3$ obtained in this study agrees very well with the linear relationship. We are therefore confident that our transition pressure is more accurate than the one observed by Lin and Liu (1997b). Studies of solid solutions between the endmembers $CaCO_3$ and $SrCO_3$ would now be very helpful to confirm the linear relationship between transition pressure and cation radius, which would then allow an extrapolation of the high-pressure phase behavior to more complex solid solutions of geophysical relevance.

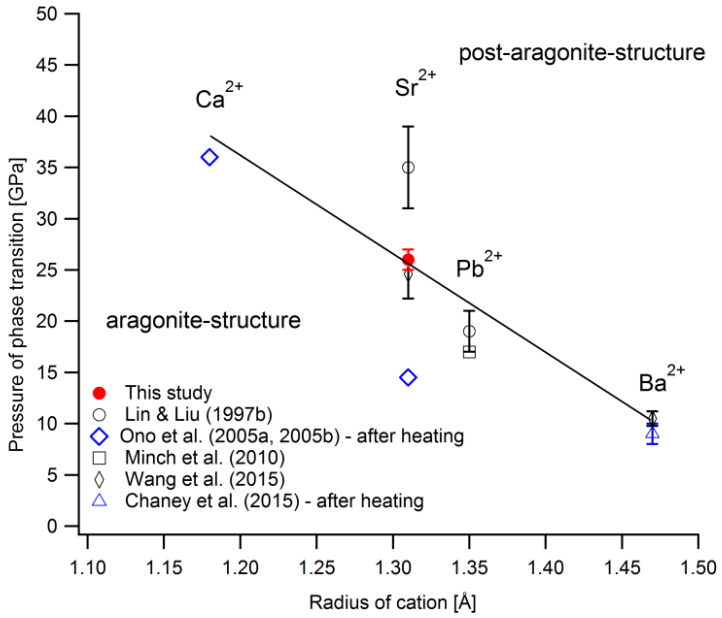

Fig. 10: Pressure of phase transition for aragonite-type $CaCO_3$, $SrCO_3$, $PbCO_3$ and $BaCO_3$ as a function of cation radius (cation radii are from Wang et al. 2015). The *line* is drawn as a guide for the eyes showing a clear negative linear dependence between cation radius and transition pressure. Note that *blue symbols* mark a pressure for the phase transition after the sample was heated up

Acknowledgements We thank Christian Schmidt for his assistance with Raman spectroscopy and all other colleagues from GFZ Potsdam who provided insights and fruitful discussions that greatly assisted the research. We also thank our reviewers for their thoughtful comments and suggestions. This study is embedded in the DFG-funded research unit FOR2125 CarboPaT (Structures, properties and reactions of carbonates at high pressures and temperatures).

References

Arapan S, Ahuja R (2010) High-pressure phase transformations in carbonates. Phys Rev B 82:184115

Bayarjargal L, Winkler B (2014) Second harmonic generation measurements at high pressures on powder samples. Zeitschrift für Kristallographie Cryst Mater 229:92–100

Biellmann C, Gillet P, Guyot F, Peyronneau J, Reynard B (1993) Experimental evidence for carbonate stability in the Earth's lower mantle. Earth Planet Sci Lett 118:31–41

Bosak A, Fischer I, Krisch M, Brazhkin V, Dyuzheva T, Winkler B, Wilson D, Weidner D, Refson K, Milman V (2009) Lattice dynamics of stishovite from powder inelastic X-ray scattering. Geophys Res Lett 36:L19309

Brenker FE, Vollmer C, Vincze L, Vekemans B, Szymanski A, Janssens K, Szaloki I, Nasdala L, Joswig W, Kaminsky F (2007) Carbonates from the lower part of transition zone or even the lower mantle. Earth Planet Sci Lett 260:1–9

Chaney J, Santillán JD, Knittle E, Williams Q (2015) A high-pressure infrared and Raman spectroscopic study of $BaCO_3$: the aragonite, trigonal and *Pmmn* structures. Phys Chem Miner 42:83–93

Clark SJ, Segall MD, Pickard CJ, Hasnip PJ, Probert MIJ, Refson K, Payne MC (2005) First principles methods using CASTEP. Zeitschrift für Kristallographie Cryst Mater 220:567–570

Dasgupta R, Hirschmann MM (2010) The deep carbon cycle and melting in Earth's interior. Earth Planet Sci Lett 298:1–13

De Villiers J (1971) Crystal structures of aragonite, strontianite and witherite. Am Miner 56:758-767

Deer WA, Howie RA, Zussman J (1992) An introduction to the rock-forming minerals. Longman Group Limited, Essex

Frech R, Wang EC, Bates JB (1980) The Ir and Raman spectra of $CaCO_3$ (aragonite). Spectrochim Acta, Part A 36:915–919

Hammouda T, Keshav S (2015) Melting in the mantle in the presence of carbon: review of experiments and discussion on the origin of carbonatites. Chem Geol 418:171–188

Kerrick DM, Connolly JA (2001) Metamorphic devolatilization of subducted oceanic metabasalts: implications for seismicity, arc magmatism and volatile recycling. Earth Planet Sci Lett 189:19–29

Kushiro I, Satake H, Akimoto S (1975) Carbonate-silicate reactions at high pressures and possible presence of dolomite and magnesite in the upper mantle. Earth Planet Sci Lett 28:116–120

Lin C-C, Liu L-G (1997a) High pressure phase transformations in aragonite-type carbonates. Phys Chem Miner 24:149–157

Lin C-C, Liu L-G (1997b) Post-aragonite phase transitions in strontianite and cerussite--a high-pressure Raman spectroscopic study. J Phys Chem Solids 58:977–987

Mao HK, Xu J, Bell PM (1986) Calibration of the ruby pressure gauge to 800 kbar under quasi-hydrostatic conditions. J Geophys Res 91:4673

Mao HK, Hemley RJ, Mao AJ (1997) Diamond-cell research with synchrotron radiation. In SK Sikka (Ed) Advances in high pressure research in condensed matter: proceedings of the international conference on condensed matter under high pressures, Nov. 11 - 15, 1996, Bhabha Atomic Research Centre, Mumbai, India, 1st ed. National Institute of Science Communication, New Delhi

Merlini M, Hanfland M, Crichton WA (2012) $CaCO_3$-III and $CaCO_3$-VI, high-pressure polymorphs of calcite: possible host structures for carbon in the Earth's mantle. Earth Planet Sci Lett 333-334:265–271

Milliman JD (1974) Marine carbonates, Part I. Springer, Heidelberg

Minch R, Dubrovinsky L, Kurnosov A, Ehm L, Knorr K, Depmeier W (2010) Raman spectroscopic study of $PbCO_3$ at high pressures and temperatures. Phys Chem Miner 37:45–56

Minsky M (1961) Microscopy apparatus. Google Patents

Monkhorst HJ, Pack JD (1976) Special points for Brillouin-zone integrations. Phys Rev B 13:5188

Müller J, Speziale S, Efthimiopoulos I, Jahn S, Koch-Müller M (in press) Raman spectroscopy of siderite at high pressure: Evidence for a sharp spin transition. American Mineralogist. doi: 10.2138/am-2016-5708

Neuhaus A (1964) Synthese Strukturverhalten und Valenzzustände der anorganischen Materie im Bereich hoher und höchster Drücke. Chimia 18:93

Nguyen-Thanh T, Bosak A, Bauer JD, Luchitskaia R, Refson K, Milman V, Winkler B (2016) Lattice dynamics and elasticity of $SrCO_3$. J Appl Cryst. doi: 10.1107/S1600576716014205

Ono S (2007) New high-pressure phases in $BaCO_3$. Phys Chem Miner 34:215–221

Ono S, Shirasaka M, Kikegawa T, Ohishi Y (2005) A new high-pressure phase of strontium carbonate. Phys Chem Miner 32:8–12

Perdew JP, Ernzerhof M, Burke K (1996) Rationale for mixing exact exchange with density functional approximations. J Chem Phys 105:9982–9985

Rappe AM, Rabe KM, Kaxiras E, Joannopoulos JD (1990) Optimized pseudopotentials. Phys Rev B 41:1227

Refson K, Tulip PR, Clark SJ (2006) Variational density-functional perturbation theory for dielectrics and lattice dynamics. Phys Rev B 73:155114

Ringwood AE (1975) Composition and petrology of the earth's mantle. McGraw-Hill, New York, p 618

Siidra OI, Krivovichev SV, Filatov SK (2008) Minerals and synthetic Pb(II) compounds with oxocentered tetrahedra: review and classification. Z Kristallogr 223:114–125

Speer JA & Hensley-Dunn ML (1976) Strontianite composition and physical properties. Am Mineral 61:1001–1004

Walker D, Carpenter MA, Hitch CM (1990) Some simplifications to multianvil devices for high pressure experiments. Am Mineral 75:1020–1028

Wang M, Liu Q, Nie S, Li B, Wu Y, Gao J, Wei X, Wu X (2015) High-pressure phase transitions and compressibilities of aragonite-structure carbonates: $SrCO_3$ and $BaCO_3$. Phys Chem Miner 42:517–527